VIII SEPOPE
19 a 23 de Maio de 2002
May - 19 st to 23 th - 2000
BRASÍLIA (DF) - BRASIL

VIII SIMPÓSIO DE ESPECIALISTAS EM PLANEJAMENTO DA OPERAÇÃO E EXPANSÃO ELÉTRICA

VIII SYMPOSIUM OF SPECIALISTS IN ELECTRIC OPERATIONAL AND EXPANSION PLANNING

IMPACT OF INDUCTION MOTOR LOADS INTO VOLTAGE STABILITY MARGINS OF LARGE SYSTEMS – RIO AREA ANALYSIS

Ricardo Mota Henriques
COPPE/UFRJ

Nelson Martins [#]
CEPEL

Júlio C. R. Ferraz
CEPEL – COPPE/UFRJ

Antônio C. B. Martins
Furnas Centrais Elétricas S.A.

Herminio José C. P. Pinto
CEPEL

Sandoval Carneiro Jr.
COPPE/UFRJ

Summary

Voltage stability margins are highly dependent on system load characteristics as well as on the modeling of the subtransmission network and associated voltage control equipment. Induction motors are loads that present high reactive power consumption during depressed voltage conditions and therefore deserve careful consideration in voltage stability studies. This paper presents continuation power flow results for the Rio de Janeiro Area, investigating the impact of induction motor loads on the system loading margins. The simulations indicated a reduction in these loading margins, better reflecting the high reactive power consumption and voltage depression conditions observed in the actual system during hot summer days.

Keywords: Voltage Collapse, Induction Motor, Load Modeling.

Introduction

The partial blackouts that occurred in the Southeast region of Brazil on April 24th and 25th 1997 were a result of voltage instability and collapse. These events occurred because the system reached its maximum loading limit and its reactive power reserves were exhausted. The analysis of these events, which also occurred in many parts of the world [1],[2], requires the development and use of adequate methodologies and efficient software. Continuation power flows have proved efficient in these studies, allowing the computation of P-V and Q-V curves, maximum loading margins, sensitivity to loading margins [3], etc.

The depressed voltage conditions that occurred several times in the Rio de Janeiro Area had active loadings below the expected critical values. However, the associated reactive loadings observed in practice were higher than expected. The higher discrepancies between the operation studies and the observed system conditions occurred during hot summer days, when the use of air-conditioning systems is intensive. This fact indicated that the common practice of representing loads by constant-P (MW) and constant-I (MW) models was not adequate, and that the induction motor loads should be better modeled.

Studies on load composition [4] revealed that motors constitute more than half of the total load, accounting for 78 % of the industrial, 37 % of residential and 43 % of the commercial energy consumption.

This paper describes the implementation of aggregate induction motor models into a continuation power flow program [5]. These motor models are classified into several types, whose typical parameters are embedded in the program code. The program user must then only specify the motor type and the motor content in each load bus or system area. The assumptions made to carry out the loadability studies of the Rio de Janeiro Area, and the main conclusions obtained are also described in the paper.

Motor modeling in power flow studies

An induction motor is characterized by both its mechanical and electrical behavior [6]. The mechanical behavior is described by the rate of change of:

$$s = \frac{w_0 - w}{w_0} \tag{1}$$

$$\frac{ds}{dt} = \frac{1}{2H}\left(T_e - T_m\right) \tag{2}$$

Where:

s – slip

---

w – rotor speed

w_0 – synchronous speed

H – inertia constant

T_m – mechanical torque

T_e – electrical torque

The mostly used steady-state model for induction motors is given by the circuit depicted in Figure 1.
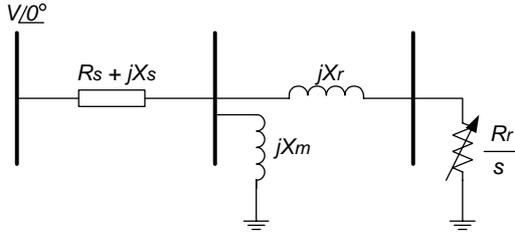

Figure 1. Classical steady-state model for induction motors.

Where:

Rs – stator resistance

Xs – stator leakage reactance

Xm – magnetizing reactance

Xr – rotor leakage reactance

Rr – rotor resistance

The 2-bus model depicted in Figure 2 is equivalent to that of Figure 1, but presents some advantages for implementation into a power flow program [7].
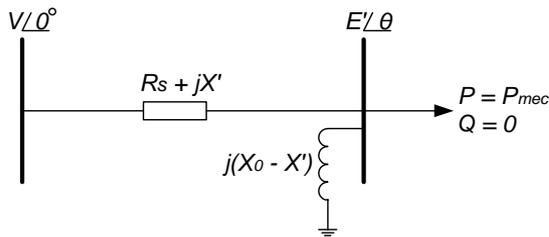

Figure 2. Two-bus steady-state model for induction motors.

Where:

P_{mec} – mechanical power

$X_0 = X_S + X_m$ – transient reactance

$X' = X_S + \dfrac{X_r \, X_m}{X_r + X_m}$ – magnetizing reactance

The model depicted in Figure 2 can be derived by different approaches. The approach described in this section is considered to be of interest. The electrical behavior of the induction motor is given by equation (3):

$$\frac{dE'}{dt} = -\frac{1}{T_0'}\left[E' - j\left(X_0 - X'\right)I_1\right] - jw_0 sE' \tag{3}$$

Where:

E' - motor transient voltage

T_0' - open circuit time constant

Figure 3 shows the induction motor equivalent circuit for both steady-state and dynamic conditions.
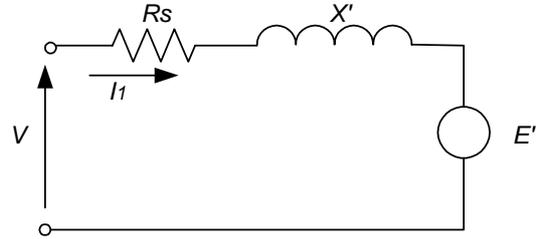

Figure 3. Induction motor dynamic equivalent circuit.

Based on the equivalent circuit of Figure 3, the current injected in the motor is given by [8]:

$$I_1 = \frac{V_t - E'}{R_S + jX'} \tag{4}$$

By setting to zero the time derivative in equation (3), one obtains the steady-state model for induction motors:

$$j\left(X_0 - X'\right)I_1 - E' - jw_0 sE'T_0' = 0 \tag{5}$$

or:

$$I_1 = \frac{E'}{j\left(X_0 - X'\right)} + E'\frac{w_0 sT_0'}{\left(X_0 - X'\right)} \tag{6}$$

Therefore, the internal voltage E' is produced by the current I_1, flowing through two parallel branches. One is purely inductive while the other is purely resistive, as shown in equation (6). These two branches are depicted in the steady-state model in Figure 4.
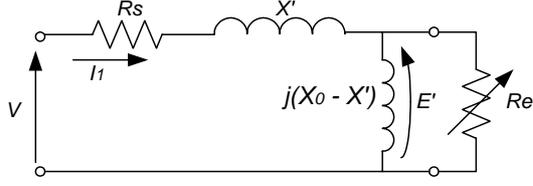
Figure 4. Steady-state equivalent circuit for induction motor.

Where:

R_e – equivalent rotor resistance

The values for R_e in Figure 4 and for P_{mec} in Figure 2 are directly obtained from equation (6):

$$R_e = \frac{(X_0 - X')}{sw_0 T'_0} \qquad (7)$$

$$P_{mec} = \frac{E'^2}{R_e} \qquad (8)$$

Figure 2 presents a model that has a two-node structure, with one node representing the motor terminals and the other representing the transient internal voltage and the mechanical torque. This can be interpreted as a two-node standard power flow problem, if the mechanical torque is assumed independent of rotor speed [9]. The following assumptions are made:

- Subtransient effects on the rotor are neglected;

- Iron core losses are neglected;

- Linear magnetic characteristic;

- Motor parameters are independent of rotor speed.

For each modeled motor, the electrical network is augmented by one bus ($P = P_{mec}$; $Q = zero$) with an additional shunt element $j(Xo – X')$ and connected to the terminal bus by an additional impedance $Rs + j\ X'$. Therefore for a system with m motors, m additional PQ buses will be created. Once the power flow solution is obtained, the rotor slip of each motor is computed using equations (7) and (8).

Table 1 lists 7 types of induction motor given in [10], [11],[12]. In the input data file for a power flow program, the bus data should indicate which motor type will be used and the percentage of load to be modeled as motors.

Table 1: Typical parameters for induction motors.

Motor Type	Motor Characteristics
1	Small Industrial I
2	Large Industrial
3	Mean values for 11 kVA motors
4	Small Industrial II
5	Commercial + feeder
6	Aggregate residential
7	Single phase

The MVA base adopted for each motor is a function of the percentage of the load modeled as motor in that particular bus. The power flow program calculates both the active and reactive consumption of the induction motor. The internal bus voltage E' and angle θ along with the rotor slip s are also computed. The remainder of the original load, which is not modeled as motor is denoted by P' and Q' in Figure 5.
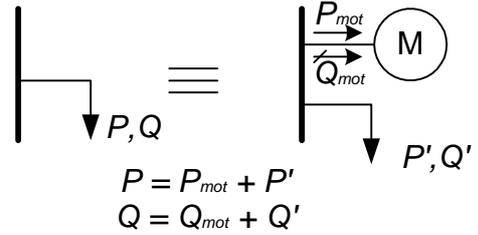

Figure 5. Initial condition for buses with induction motor loads.

In the continuation power flow studies, the induction motor load is increased by conveniently increasing the MVA motor base. This procedure is equivalent to increasing the number of motors in the system.

Illustrative example

A two-bus system was used in order to validate the implementation of the models for induction motor in a power flow program. The continuation power flow was used to obtain the maximum loadability of the test system for different models of the load at bus #2 (Figure 6). The models used were:

- Constant P, no reactive power consumption;

- Induction motor (Small Industrial II and Commercial+Feeder, see Table 1).

The maximum loadability was computed for different load models. The percentage of motor load was also varied (100%, 90% and 80%). Figure 7 presents the PxV curves for the seven load compositions analyzed.
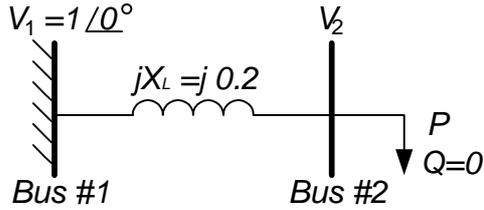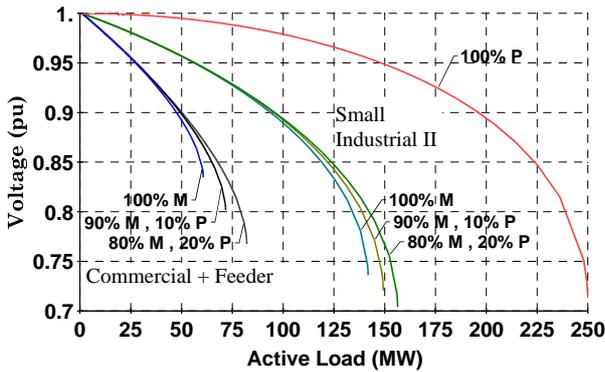
Figure 6. Test System.

Figure 7. PxV curves for different load models at bus #2.

Figure 8 and Figure 9 show the reactive power consumption and rotor slip the induction motor load of two types. Note the two types of motor show rather different performances, the Commercial+Feeder type causing a larger reduction to the system loading margin.
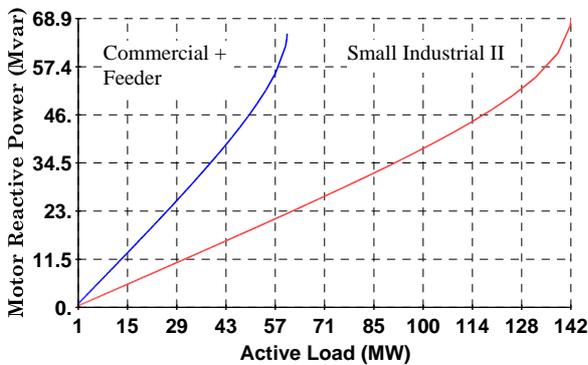

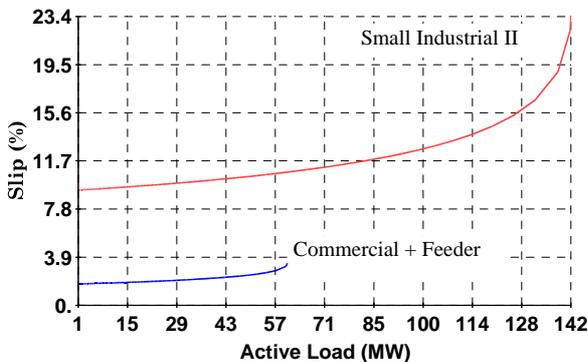Figure 8. Reactive power consumption at bus #2.

Figure 9. Rotor Slip curves for two set of induction motor parameters.

Maximum Loadability Assessment of the Rio Area

The maximum loadability assessment of the Rio Area is carried out in this section. The Rio Area is a part of the Brazilian interconnected system containing three utilities: LIGHT, CERJ and ESCELSA. The Rio Area has 288 buses, out of which 200 are load buses (7632 MW). There are 149 buses with a high motor content non-zero load and are modeled as induction motor (5733 MW). The system model utilized has 2953 buses (51175 MW). The operation point refers to a heavy load condition for the Rio Area on a summer working day of the year 2002.

Table 2 presents load data information the regarding the number of buses with motors and the percentage of motor content in these buses. The most relevant residential load buses are included in the buses classified as Commercial on Table 2.

Table 2: Buses with load modeled as induction motors.

Region	Number of Buses with motors	Percentage of Bus Load Modeled as Motor	
		Commercial	Industrial
Barra/Jacar.	8	80	20
Centro	5	90	10
Ilha do Gov.	4	50	10
Leopoldina	9	55	45
Méier/Casc.	7	75	25
Nova Iguaçu	19	70	30
Tijuca	4	80	20
Triagem	3	50	50
Vale	9	70	30
Zona Oeste	12	70	30
Zona Sul	10	90	10
Industrial	12	-	100
CERJ 1	4	33	-
CERJ 2	5	-	33
CERJ 3	4	50	-
CERJ 4	2	-	50
CERJ 5	7	100	-
CERJ 6	2	-	100
ESCELSA 1	3	33	-
ESCELSA 2	4	50	-
ESCELSA 3	5	-	50
ESCELSA 4	3	100	-
ESCELSA 5	8	-	100
TOTAL	149		

Other assumptions made in the continuation power flow analysis are described below. The motor load classified

4

as Industrial (see Table 2) remains constant and only the load classified as Commercial (Table 2) is increased.

The Commercial load is initially modeled as constant P and Q, with fixed power factor. The Industrial load is also modeled as constant P and Q however, as previously stated, its magnitude remains fixed. Figure 10 shows the PxV curves for the three most critical buses, all of them belonging to ESCELSA (one of the three distribution utilities in the Rio Area).
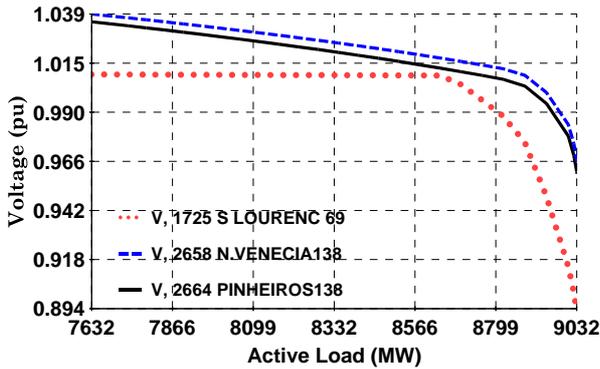

Figure 10. Rio Area load increase (constant P and Q load model).

Two cases were investigated where the Commercial load (Table 2) was modeled by either: Commercial+Feeder or Small Industrial II (Table 1). The Industrial motor load (Table 2) is modeled as Large Industrial (Table 1), but kept fixed at the base case value. The maximum loadability curves for these two motor load modeling alternatives are shown in Figure 11 and Figure 12.
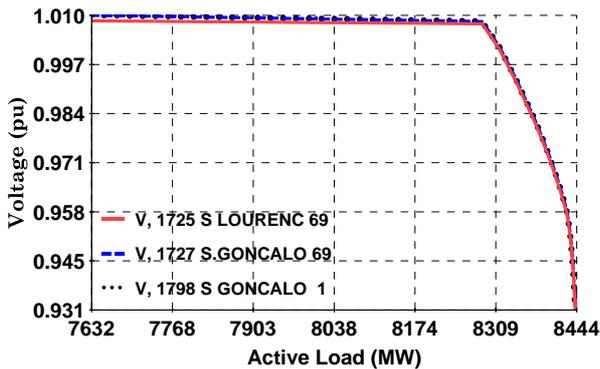

Figure 11. Rio Area load increase (Commercial induction motor modeled as type 5: Commercial+Feeder).
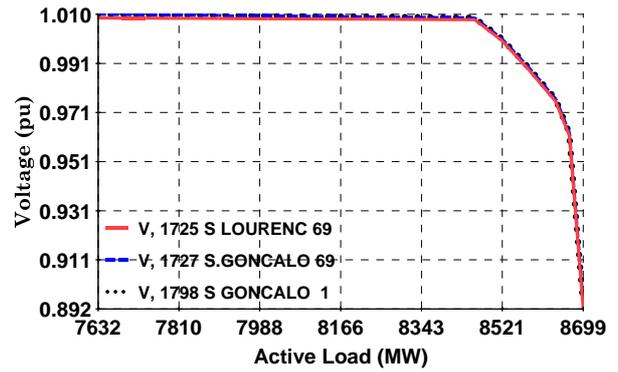

Figure 12. Rio Area load increase (Commercial induction motor modeled as type 4: Small Industrial II).

The loading margin in the Rio Area is always restricted by the maximum limits of the reactive power sources being reached, regardless the load model used. There are, nevertheless, important differences to be pointed out. When the model used is constant P and Q, the critical buses are those in a radial area of ESCELSA. The nose curve for "Pinheiros 138 kV" bus voltage (Figure 10), clearly indicates that the lack of reactive power occurred near to the network natural maximum loadability value (no bounds or Q-limits).

When the load is represented as induction motor models, the loading margin is considerably smaller. The critical buses in this case have induction motors and are located in commercial and residential areas fed by a rather meshed network (Figure 11 and Figure 12).

The modeling of induction motors in the Rio Area causes reduction of 588 MW in the loading margin. The maximum loadability decreases from 9032 MW (Figure 10) to 8444 MW (Figure 11) or 8699 MW (Figure 12). These results are summarized in Table 3.

Figure 13 and Figure 14 allow the comparison of the three scenarios analyzed. The PxV curves presented relate to two of the most critical system buses: "Pinheiros 138 kV" (ESCELSA) and "S Lourenc 69 kV" (CERJ).

Table 3: Maximum loadability for 3 different load models.

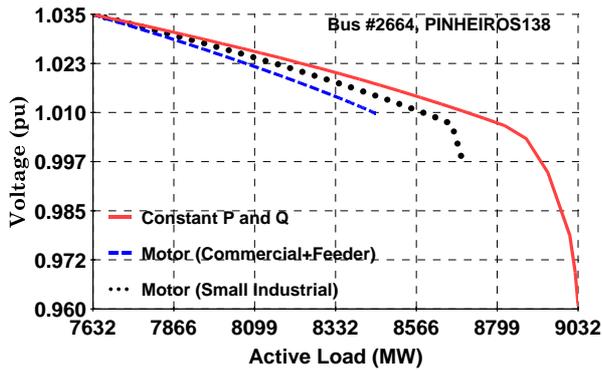| Load Model	Rio Area ActiveLoad		
	Initial Load (MW)	Induction Motor (MW)	Maximum Loadability (MW)
Constant P and Q	7632	-	9032
Induction Motor 4 (Table 2)	7632	5733	8699
Induction Motor 5 (Table 2)	7632	5733	8444

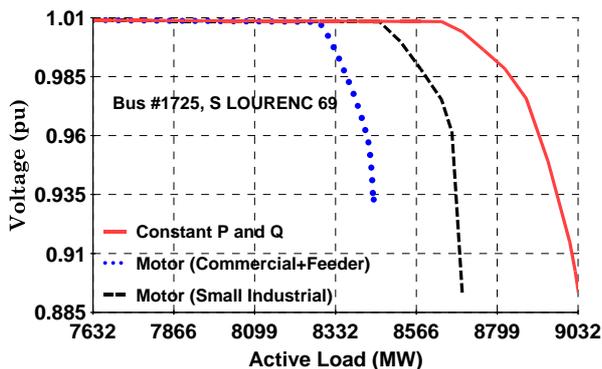Figure 13. PxV curves of "Pinheiros-138 kV" for 3 scenarios.

Figure 14. PxV curves of "S Lourenc-69 kV" for 3 scenarios.

Conclusions

The adequate modeling of induction motor loads into continuation power flow programs may better reproduce system behavior and reveal voltage stability problems. Finding the cost-effective level of modeling for subtransmission and distribution networks is not an easy task.

After judicious modeling of motor load content into 106 load buses, the maximum loadability studies indicated that town centers of the Niteroi and Rio de Janeiro cities have buses with very depressed voltages. These results are in line with observed system behavior, and would not be obtained if only constant-P and constant-I load models were utilized.

One must note that the continuation power flow results for the illustrative system of Section 3 did not consider reactive power limits. These limits are however always reached in practical systems as the loading level is raised, as demonstrated in the results described for the Rio Area.

Acknowledgements

References

[1] Y. Mansour - Editor, "Suggested Techniques for Voltage Stability Analysis", IEEE/PES Special Publication, 93TH0620-5PWR, Piscataway, NY, 1993.

[2] C. Cañizares - Editor, "Voltage Stability", IEEE/PES Special Publication, December 2000, available at

http://www.power.uwaterloo.ca/~claudio/.

[3] S. Greene, I. Dobson, F.L. Alvarado, "Sensitivity of The Loading Margin to Voltage Collapse With Respect to Arbitrary Parameters", IEEE Transactions on Power Systems, v. 12, n. 1 (February), pp. 262-272, 1997.

[4] C.W. Taylor, Power System Voltage Stability, McGraw-Hill Inc, 1994.

[5] H.J.C.P. Pinto, J.L.R. Pereira, N. Martins, J.A.P. Filho, S.G. Junior, F.R.M. Alves, J.C.R. Ferraz, R.M. Henriques and V.M. Costa, "Needs and Improvements in Power Flow Analysis", Proceedings of the VII SEPOPE, Curitiba, PR, May 2000.

[6] IEEE Task Force on Load Representation for Dynamic Performance, "Standard Load Models for Power Flow and Dynamic Performance Simulation", IEEE Transactions on Power Systems, Vol. 10, No. 3, August 1995.

[7] B. Stott, "User's Manual for Load Flow Program", UMIST, UK, 1974.

[8] A.S. Pedroso, "Induction Motor – Mathematical Modeling Including Rotor Transients", CEPEL Technical Report No. 305, Rio de Janeiro, RJ, Brazil, 1987 (in Portuguese).

[9] E. Bompard, E. Carpaneto, G. Chicco and R. Napoli, "Asynchronous Motor Models for Voltage Stability Analysis", Proceedings Bulk Power System Voltage Phenomena III – Voltage Stability Security and Control, ECC Inc, Davos, Switzerland, August 1994.

[10] P. Kundur, Power System Control and Stability, McGraw-Hill Inc, USA, 1994.

[11] T. Van Cutsem and C. Vournas, Voltage Stability of Electric Power Systems, Kluwer Academic Publishers, 1998.

[12] G.J. Rogers Nozari, J. Manno and R.T.H. Alden, "An Aggregate Induction Motor Model for Industrial Plants", IEEE Transactions on Power Systems, Vol. PAS-103, No. 4, April 1984.